

Correspondence

A Framework for Predictive Modeling of Anatomical Deformations

Christos Davatzikos, Dinggang Shen, Ashraf Mohamed, and Stelios K. Kyriacou

Abstract—A framework for modeling and predicting anatomical deformations is presented, and tested on simulated images. Although a variety of deformations can be modeled in this framework, emphasis is placed on surgical planning, and particularly on modeling and predicting changes of anatomy between preoperative and intraoperative positions, as well as on deformations induced by tumor growth. Two methods are examined. The first is purely shape-based and utilizes the principal modes of co-variation between anatomy and deformation in order to statistically represent deformability. When a patient's anatomy is available, it is used in conjunction with the statistical model to predict the way in which the anatomy will/can deform. The second method is related, and it uses the statistical model in conjunction with a biomechanical model of anatomical deformation. It examines the principal modes of co-variation between shape and forces, with the latter driving the biomechanical model, and thus predicting deformation. Results are shown on simulated images, demonstrating that systematic deformations, such as those resulting from change in position or from tumor growth, can be estimated very well using these models. Estimation accuracy will depend on the application, and particularly on how systematic a deformation of interest is.

Index Terms—Deformable models, intraoperative deformation, soft tissue deformation, surgical planning.

I. INTRODUCTION

Modeling anatomical deformations is becoming increasingly important in image-guided surgery. Anatomical deformations might be due to diverse factors such as changes in patient positioning, needle puncturing, skull opening, tumor growth, or natural bone growth after reconstructive surgery. Many of these deformations can be predicted to a large extent by statistical or biomechanical deformable models. The former require that the deformation of interest can be observed in a number of cases, which are treated as training samples from which a statistical predictive model is built. The latter are based on knowledge of the biomechanical behavior of biological tissues.

A number of investigators have used biomechanical models to predict intraoperative deformations, particularly with respect to brain shift during image-guided neurosurgery [1]–[4]. Biomechanical models have also been used to model deformations induced by various pathologies such as tumor growth [5], [6], edema [7]–[9], hydrocephalus [10], [11], and intracerebral hematoma [12], as well as for

traumatic injury [13]–[18]. Several other studies have focused more generally on modeling material properties of soft tissue [19]–[24].

Biomechanical models represent an important aspect of deformable modeling, since they utilize physical knowledge about properties of deformable organs. However, they have two limitations. First, they require that material properties, constitutive equations, and boundary conditions are known. This is rarely the case, particularly with respect to boundary conditions. (Modeling brain shift is perhaps one of the very few exceptions, since it is greatly facilitated by the rigid skull and the easily modeled effect of gravity.) Second, they are computationally very demanding.

An alternative approach is based on statistical modeling utilizing a number of training samples for which the deformation is known [25], [26]. For example, in [26] the growth of the mandible was measured from images of a number of children. The statistical properties of the underlying growth field were examined via principal component analysis, and the principal eigenvector that reflected a large percentage of the variation of the growth field was used to predict the direction of growth. Related are a number of statistical shape models [27]–[30] that use principal component analysis in the context of segmentation and template matching. These models are not concerned with prediction *per se*, but rather with modeling normal anatomical variability for the scope of shape segmentation and quantification.

In this paper, we describe a framework for modeling and predicting deformations, which has two novel contributions. First, it examines not only the principal modes of variation of shape [27] or deformation [26], but also the principal modes of co-variation between shape and deformation. Therefore, anatomical information collected from a particular patient's images can contribute to a more accurate prediction of how the patient's anatomy will deform, compared to prediction based only on statistical properties of the underlying deformation field [26]. Second, we present an approach for incorporating biomechanical knowledge into the statistical predictive model, thereby capturing the nonlinear biomechanical behavior of soft tissue.

In our framework, we assume that the deformation of interest is known for a number of cases that are used as training samples. Training samples can be obtained in one of two ways, leading to two different, but related methods for predictive modeling. The first one is referred to as *shape-based estimation* (SBE). In this method, from the training set we find the principal modes of co-variation between shape and deformation, by applying principal component analysis on vectors that hold jointly landmark coordinates and their respective displacement vectors. When presented with a new shape, which corresponds to the anatomy of a patient, we express the shape in terms of the principal eigenvectors via an optimization procedure. We, thus, simultaneously obtain the most likely deformation of the individual anatomy. Our goal here is to find the component of the deformation that can be predicted from the patient's anatomy, based on the premise that anatomy (e.g., bone, muscle, ligaments) to some extent determines or constrains possible deformations.

The second approach that we examine is referred to as *force-based estimation* (FBE). It is based on the premise that often there is additional knowledge about the biomechanical properties of the deforming anatomy, which can be utilized to obtain an estimate of the deformation field. Accordingly, we find the modes of co-variation between shape and forces, rather than between shape and deformation. (Forces are calculated from the observed deformation and elastic properties; the latter

Manuscript received March 12, 2001; revised May 2, 2001. This work was supported in part by a grant from the National Science Foundation (NSF) to the Engineering Research Center for Computer Integrated Surgical Systems and Technology. The Associate Editor responsible for coordinating the review of this paper and recommending its publication was M. W. Vannier. *Astreisk indicates corresponding author.*

*C. Davatzikos is with the Center for Biomedical Image Computing, Department of Radiology, JHOC 3230, Johns Hopkins University School of Medicine, 601 N. Caroline Street, Baltimore, MD 21287 USA (e-mail: hristos@rad.jhu.edu).

D. Shen, A. Mohamed, and S. K. Kyriacou are with the Center for Biomedical Image Computing, Department of Radiology, Johns Hopkins University School of Medicine, Baltimore, MD 21287 USA.

Publisher Item Identifier S 0278-0062(01)06587-9.

are optimized for best prediction of deformation in the training set.) The deformation field is then calculated by applying the resulting forces to a finite element (FE) biomechanical model of the anatomy. One additional advantage of FBE is that it calculates displacements everywhere in the interior of a structure, and not only on the boundaries being modeled.

At this stage of our work, we have not applied our methods to a particular application, but we have created simulated shapes and deformations, in order to test and compare our methodologies. We are currently in the process of applying this method to a variety of clinical applications, including modeling the deformation of the prostate between the preoperative and intraoperative positions, and statistically characterizing soft tissue deformation caused by tumor growth.

II. METHODS

In this section, we first describe our framework for parameterizing the statistical properties of shape deformability, which is based on principal component analysis. Next, we describe our approach for predicting the deformation, based in part on the patient's anatomy and in part on the statistical model of shape deformability. Finally, we extend this framework to incorporate biomechanical properties of the deforming anatomy.

A. Statistical Model of Shape Deformability

Assume that a collection of points, perhaps landmarks, defining a shape are arranged in a vector \mathbf{s} (see Fig. 1). Consider, also, an associated vector, \mathbf{q} , which will be used to represent the deformation of the shape \mathbf{s} . The vector \mathbf{q} can have different forms, as will be elaborated later in this section. In its simplest form, it comprises a number of displacement vectors defined on their respective landmarks. In another form, it comprises forces, which applied to a biomechanical model of anatomical deformation yield displacements. Consider the vector \mathbf{x} , created by concatenating \mathbf{s} and \mathbf{q} . Our assumption is that \mathbf{x} follows a multivariate Gaussian distribution, with density $f(\mathbf{x})$ that is parameterized by its mean

$$\mu = \begin{bmatrix} \mu_s \\ - \\ \mu_q \end{bmatrix}$$

and its covariance matrix

$$\mathbf{C} = \begin{bmatrix} \mathbf{C}_{ss} & \mathbf{C}_{sq} \\ \mathbf{C}_{sq} & \mathbf{C}_{qq} \end{bmatrix}.$$

The probability density function (pdf) $f(\mathbf{x})$, or equivalently μ and \mathbf{C} that parameterize it, can be estimated from a set of cases in which the patient's anatomy, and the way in which this anatomy deforms, are both known. In that case, a number of vectors $\mathbf{x}_i, i = 1, \dots, K$, are used to calculate μ and \mathbf{C} . As we discussed in Section I, there are two ways for obtaining these samples.

Let the eigenvectors of \mathbf{C} be denoted by

$$\mathbf{v}_i = \begin{bmatrix} \mathbf{v}_{s_i} \\ - \\ \mathbf{v}_{q_i} \end{bmatrix}, \quad i = 1, \dots, K-1$$

where \mathbf{v}_{s_i} and \mathbf{v}_{q_i} are the parts of \mathbf{v}_i corresponding to \mathbf{s} and \mathbf{q} , respectively. Then, \mathbf{x} can be parameterized as follows:

$$\mathbf{x} = \mu + \sum_{i=1}^M \alpha_i \mathbf{v}_i, \quad M \leq K-1 \quad (1)$$

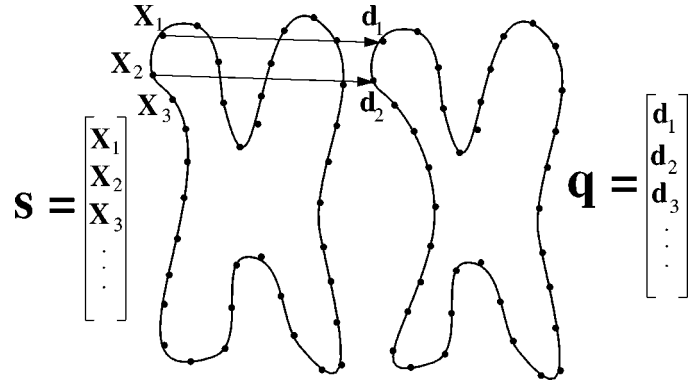


Fig. 1. A schematic diagram showing a number of landmarks that comprise the vector \mathbf{s} which represents a patient's anatomy. The vector \mathbf{q} in this figure holds the respective displacement vectors.

from which it follows that

$$\mathbf{s} = \mu_s + \sum_{i=1}^M \alpha_i \mathbf{v}_{s_i} \quad (2a)$$

$$\mathbf{q} = \mu_q + \sum_{i=1}^M \alpha_i \mathbf{v}_{q_i}. \quad (2b)$$

The vectors \mathbf{s} and \mathbf{q} are then represented entirely by $\alpha_i, i = 1, \dots, M$, provided that the mean, μ , and the eigenvectors of the covariance matrix, \mathbf{C} , of $f(\mathbf{x})$ have been determined from the training set. Equation (1) can be written in a more compact form as:

$$\mathbf{x} = \mu + \mathbf{V}\mathbf{a} \quad (3)$$

where

$$\mathbf{a} = [\alpha_1, \dots, \alpha_M]^T$$

and \mathbf{V} is a matrix containing the eigenvectors of \mathbf{C} that correspond to the M largest eigenvalues.

The pdf of the coefficient vector \mathbf{a} is given by

$$g(\mathbf{a}) = c \exp \left\{ - \sum_{i=1}^M \frac{\alpha_i^2}{2\lambda_i} \right\} \quad (4)$$

where λ_i denotes the i th eigenvalue of \mathbf{C} , and c is a normalization constant.

B. Training

In order to estimate the statistical parameters (mean and covariance matrix) of the previous section, we need a number of training samples for which the vector \mathbf{x} is known, i.e., samples for which both the shape and its deformation are known. Training samples can be obtained in one of the following two ways.

- 1) The undeformed and deformed configurations of a patient's anatomy can be captured by tomographic imaging. For example, if high-quality intraoperative imaging is available, preoperative and intraoperative images of a number of patients can be used to build a statistical model linking patient anatomy with its possible deformations. An example of a systematic deformation is in prostate brachytherapy, where the patient changes from the preoperative supine position to the intraoperative lithotomy position. Significant changes in the shape of the prostate and the surrounding anatomy can render the preoperative plans inaccurate. In order to extract the shapes of interest from tomographic images, we can use an adaptive-focus deformable

shape model (AFDM) described in detail in [31] and [29]. Point correspondences in AFDM are determined primarily via a similarity in a set of geometric attributes, which characterize the shape from a local and fine scale to a global and coarse scale.

- 2) Conceptually, using real patient images, as described above, is the most straightforward way of developing a statistical model of deformation. However, from a practical perspective, it is limited in two ways. First, for many types of anatomical deformations, a prohibitively large number of patient images would be needed to train a statistical model. An example is deformability of the spine, where one would need at least 20 or so patients, each of which would need to be scanned in tens or even hundreds of different positions, so that the normal range of variation in deformability of the spine can be captured by a statistical model. Second, it is often impossible to obtain images from both the undeformed and the deformed configuration of the anatomy. For example, if one is interested in statistically characterizing the deformation induced by tumor growth, it is very unlikely that a large enough number of patients can be found that have been scanned both before and after the tumor growth. In order to overcome these limitations, we can generate a very large number of training samples via statistical sampling, in conjunction with a biomechanical model. For example, one can start with a number of normal spine images, build biomechanical models based on properties of bone and soft tissue, and deform these models in many possible ways, each time generating a pair of (shape, deformation). These pairs can be used as training samples for a statistical model. For a new patient, the statistical model can serve as a statistical prior in predicting or tracking deformations, perhaps in conjunction with limited intraoperative data such as fluoroscopic (or ultrasound, in many applications) images. Similarly, one can simulate the growth of the tumor in a number of normal images, thus generating training samples obtaining both the pre-tumor and posttumor anatomy. In Section III, we show how this training set can be used to build an estimator of the anatomy of a tumor patient prior to the growth of the tumor.

C. Predicting \mathbf{q}

The procedure described above effectively determines not only the main modes of variation of \mathbf{s} and \mathbf{q} , but also the main modes of co-variation between \mathbf{s} and \mathbf{q} . Therefore, if \mathbf{q} is to be predicted, or to be estimated under partial or noisy information, the statistical knowledge determined in the previous section can be used as a statistical prior. Let us assume that \mathbf{q} represents the deformation between a patient's preoperative and intraoperative positions. Let the patient's preoperative anatomy, as determined from the patient's images, be represented by the vector \mathbf{s}_o . At this point we will assume that \mathbf{s}_o is accurately observed, although our formulation can be easily extended if only a noisy or incomplete observation of \mathbf{s}_o is available. Knowing \mathbf{s}_o , our goal is to predict the vector \mathbf{q} , which will determine the deformation for this patient, and therefore the patient's deformed anatomy. Since we know \mathbf{s}_o , we can express it in terms of the eigenvectors and the coefficients vector, \mathbf{a} , as in (2a). Typically, if an orthogonal basis is available, the coefficients of expansion in terms of the vectors of that basis are found by projection. However, $\{\mathbf{v}_i\}$ form a basis for the entire vector \mathbf{x} , not for the truncated vector \mathbf{s} . Therefore, projection on $\{\mathbf{v}_i\}$ is not possible. Projection on $\{\mathbf{v}_{s_i}\}$, the truncated eigenvectors, will not provide the correct coefficients vector either, since $\{\mathbf{v}_{s_i}\}$ do not form an orthogonal basis. Therefore, in order to find the vector \mathbf{a} which represents an expansion of \mathbf{s}_o in terms of $\{\mathbf{v}_{s_i}\}$, we solve an optimization problem in which \mathbf{a} is found so that it yields a shape that fits \mathbf{s}_o and that has high likelihood, the latter being expressed by $g(\mathbf{a})$ as in (4).

Specifically, for a given \mathbf{s}_o , we find the vector \mathbf{a} that minimizes the following objective function:

$$\begin{aligned} \mathcal{E}(\mathbf{a}) &= \|\mathbf{s} - \mathbf{s}_o\|^2 + w \frac{1}{g(\mathbf{a})} \\ &= \left\| \mu_s + \sum_{i=1}^M \alpha_i \mathbf{v}_{s_i} - \mathbf{s}_o \right\|^2 + w \frac{1}{g(\mathbf{a})} \end{aligned} \quad (5)$$

where w is a relative weighting factor. The first term in (5) seeks vectors that get as close as possible to the patient's observed undeformed anatomy, \mathbf{s}_o , whereas the second term favors shape representations as in (2a) that are likely, according to what has been observed in the training samples. The solution is found using the Levenberg–Marquardt [32] nonlinear optimization scheme.

Let $\hat{\mathbf{a}}$ be the vector minimizing $\mathcal{E}(\mathbf{a})$, and let it be expressed as

$$\hat{\mathbf{a}} = [\hat{\alpha}_1, \dots, \hat{\alpha}_M]^T.$$

Therefore, our estimate of \mathbf{s}_o is given by

$$\hat{\mathbf{s}}_o = \mu_s + \sum_{i=1}^M \hat{\alpha}_i \mathbf{v}_{s_i}. \quad (6)$$

At this point, we have determined the coefficients of expansion in (1) and (2a). Therefore, applying them to (2b) readily yields an estimate of the unknown deformation field

$$\hat{\mathbf{q}}_o = \mu_q + \sum_{i=1}^M \hat{\alpha}_i \mathbf{v}_{q_i}. \quad (7)$$

In summary, the expansion of \mathbf{x} in terms of the eigenvectors $\{\mathbf{v}_i\}$ is determined from the part of \mathbf{x} that is known, namely \mathbf{s}_o , and is subsequently applied to the part that is not known, namely \mathbf{q}_o .

D. Shape- and Force-Based Estimation

In what we described earlier, the predicted vector \mathbf{q} represented the deformation field. We refer to this method as *shape-based estimation*, since it treats anatomical structures as shapes. An alternative method that we examine next uses boundary forces in place of \mathbf{q} , and will be referred to as *force-based estimation*. The premise in FBE is that, if the biomechanical behavior of an organ of interest can be modeled, then it could be included in the process of estimating the deformation field. For example, if our goal is to model deformations of the prostate between the preoperative and intraoperative positions, then we would like to include into our modeling basic facts about the elastic behavior of the prostate, such as the differences in the elastic properties of the central and peripheral zones.

One could argue that if the biomechanical behavior of a structure of interest is known, then its deformation can be modeled entirely via a biomechanical FE model. However, this is not the case, in general. The forces that would be required to drive such a biomechanical model are not known, and cannot be easily modeled due to the complexity of the human anatomy and physiology, and also due to the fact that only limited coverage of the anatomy around a structure or organ of interest is typically provided by the patient's images.

In order to incorporate biomechanical knowledge into our estimation process, we developed the FBE method. The basic principle of FBE is that the forces that need to be applied to the boundary of an anatomical region, which might include an organ or a collection of organs, can form the vector \mathbf{q} , which is estimated as above. The estimated forces are then fed into a biomechanical model of the anatomical region of interest, thereby providing the required deformation field.

Unlike SBE, in which the vector \mathbf{q} that represented displacements was known in the training set, in FBE this is not the case, since no force measurements are typically provided by tomographic imaging. Forces could be computed from the known boundary displacements, by solving the associated boundary value problem, if the elastic properties of the structures of interest were known. Since, however, the range of elastic parameters that is often found in the biomechanics literature can only be viewed as approximate, in our approach we have chosen to estimate these elastic properties from the training set along with \mathbf{q} , so that optimal prediction is achieved in the training set. This leads to the following iterative algorithm.

- Step 0) Use AFDM to segment the structures of interest in sample images, and to determine point correspondences. Displacement fields are obtained readily from the point correspondences.
- Step 1) Based on a rough estimate of the elastic properties of the structures of interest, and on the available displacement fields of the training samples, calculate the force distribution along the boundaries of the anatomical regions of interest, using an FE biomechanical model. This step is straightforward, since knowledge of displacements and elastic parameters leads directly to estimates of stresses and boundary forces everywhere.
- Step 2) Leave one of the training samples out. Set $\mathbf{q} =$ calculated boundary forces for the remaining training samples. For the left out sample, determine the statistical estimator of \mathbf{q} , given \mathbf{s} , as described in Section II-C (see (7)).
- Step 3) Test the estimation accuracy on the left out sample. In particular, apply the estimated \mathbf{q} to the biomechanical model, thereby obtaining an estimate of the displacement field. Estimated displacement fields are then compared with true displacement fields, which are known from Step 0 for these training samples.
- Step 4) Repeat Steps 2 and 3 for each training sample, each time calculating the estimation error. Compute the average estimation error over all the training samples.
- Step 5) If the error has converged then stop. Otherwise, update the elastic parameters based on the gradient of the average estimation error and go to Step 1.

This procedure determines estimates for two sets of variables: 1) optimal elastic parameters, 2) variables of the predictive model (the set $\mathbf{v}_i, i = 1, \dots, M$ corresponding to the optimal elastic parameters). When presented with a new patient (i.e., the preoperative anatomy of the patient), we use the predictive model to obtain force estimates. We then feed these estimated forces into the FE mesh created for that patient, and by using the elastic parameters determined from the training set, we calculate the displacement field, and therefore the deformed anatomy.

Internal Forces: In the presentation of FBE, we have restricted our discussion to boundary forces. It should be noted that this does not necessarily imply that our method is only applicable to problems that involve this kind of forces. Known internal forces, such as gravity, can be added to the FE model, thus providing the capability of incorporating effects induced by such forces. The density of the tissue is approximately known and the direction of gravity would be known for both the preoperative and intraoperative positions. In contrast, the handling of the so-called residual stresses within the tissue due to swelling effects would be rather more difficult to handle since it would require quantification of these stresses. Further research will be needed to elucidate the effect of these residual stresses in our methodology.

Our premise with the use of boundary forces in FBE is that one can focus on a region of interest (ROI) and model how surrounding regions affect the deformation in this ROI. Referring to the example of

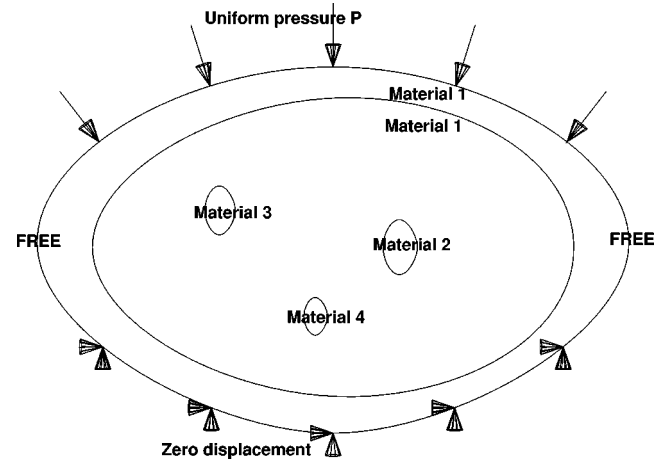


Fig. 2. The model used as computational phantom in our first experimental study. Uniform pressure was applied at the top and fixed boundary conditions were applied at the bottom of the large ellipse. Each ellipse had its own elastic properties. Deformations were simulated using FEs with linear elasticity but nonlinear kinematics.

the prostate, one might want to focus only on the deformation of the prostate anatomy between the preoperative supine position and the intraoperative lithotomy position. The underlying forces that are responsible for this deformation are very complex and difficult to model. For example, in the lithotomy position, the weight and repositioning of the legs causes deformation which eventually propagates to the prostate via other structures. To add to this complexity, the whole body anatomy is not even known for a patient, since much of it is outside the field of view of the scanner, thus precluding the use of a biomechanical model for estimating deformations. In the previous discussion, our assumption has been that one can isolate the prostate as the ROI, and knowing that it is composed of elastic soft tissue, one can model its deformation caused by forces exerted on it by surrounding tissue, no matter what the actual origin or distribution of these forces is.

III. RESULTS

We performed two kinds of experiments, both using simulations of mechanical deformations. The first experiment was motivated by the potential use of our predictive framework in estimating deformations between the preoperative and intraoperative positions. The second experiment was motivated by potential uses of our framework in modeling soft tissue deformation under growing tumors. In both experiments, simulated deformations were generated via an FE model.

A. Experiment 1

We considered a synthetic shape comprising five ellipse-like areas (see Fig. 2). Each ellipse represents a different anatomical region with its own elastic properties. The material behavior is assumed to be linear elastic with a Poisson ratio equal to 0.48, which gives an almost incompressible behavior typical of soft tissues. The Young's moduli, denoted by E_i for the i th ellipse, are within the range of the Young's moduli of soft tissue (order of $10\,000\text{ N/m}^2$).

In order to simulate deformation, we applied uniform pressure at the top and fixed boundary conditions at the bottom (see Fig. 2). Linear elasticity is not necessary but is just a convenient first approximation. ABAQUS/CAE [33] was used for the automatic creation of the geometry, the application of elastic properties and boundary conditions, meshing, and the solution of the resulting FE model. Although linear materials were used, large deformation mechanics rendered the problem nonlinear.

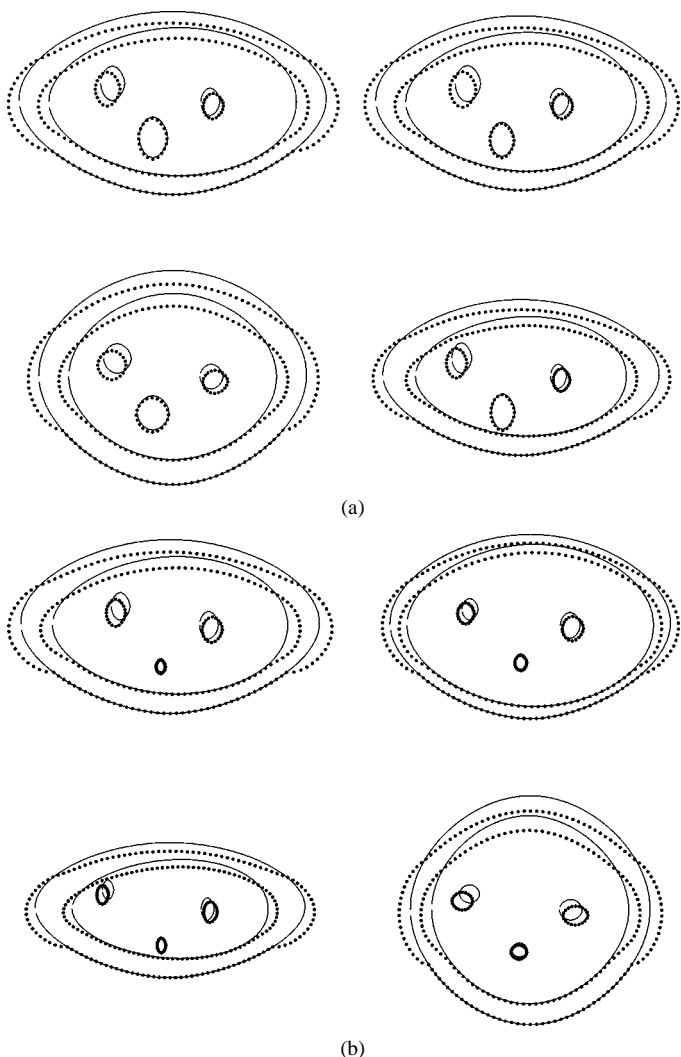


Fig. 3. Four example simulated shapes resulting from statistically sampling the distribution of the ellipses and applying the mechanical model of Fig. 2. (a) Relatively lower parameter variation. (b) Relatively higher parameter variation. Solid lines denote the undeformed configurations while dotted lines denote the deformed configurations.

In order to simulate variability in shape and loading conditions, we used statistical sampling for all major parameters of the simulated training samples: pressure at the top, major and minor diameters for all ellipses, the Young's moduli, and positions of the three small ellipses. We created two sets of training samples, having relatively lower and relatively higher variation in parameters. The first training set included 20 samples and the second one included 40 samples. Their parameters were drawn from Gaussian distributions having standard deviations $1/20$ and $1/10$, respectively, of the absolute values of the parameters. Four typical sample shapes from the first sample set (relatively lower parameter variation) are shown in Fig. 3(a), illustrating the extent of variation in the samples. Four typical sample shapes from the second sample set (relatively higher parameter variation) are shown in Fig. 3(b).

In order to test our predictive model, we used the "leave-one-out" method. In particular, we randomly selected five of the 20 training samples and used each one of them as test sample. Each time the remaining 19 samples were used to train the predictive model. The following estimates were used for the elastic properties for FBE: $E_1 = E_{1\text{mean}} * 2$, $E_2 = E_{2\text{mean}} * 0.5$, $E_3 = E_{3\text{mean}} * 2$, $E_4 = E_{4\text{mean}} * 0.5$. By $E_{1\text{mean}}$, $E_{2\text{mean}}$, \dots , etc., we denote the mean values of the Gaussian

TABLE I

NORMALIZED ERRORS OBTAINED FOR FIVE TARGETS FROM THE TRAINING DATASET WITH RELATIVELY LOWER PARAMETER VARIATION. EACH ROW CORRESPONDS TO A DIFFERENT SAMPLE USED FOR EVALUATION BY THE "LEAVE-ONE-OUT" METHOD. THE MEAN FOR SBE WAS $0.085 = 8.5\%$ AND THE MEAN FOR FBE WAS $0.08 = 8\%$

Error in SBE	Error in FBE
0.115256	0.054368
0.047286	0.066952
0.065547	0.056310
0.081303	0.070515
0.116419	0.133702

distributions from which the Young's moduli of the training dataset were sampled. The subscript 1 denotes the two largest elliptical regions, whereas 2, 3, and 4 denote the small internal elliptical regions. By using material properties different than the true (mean) ones, we wanted to test the robustness of our predictive model to substantially different estimates of the elastic parameters. (Note that these elastic parameter estimates are only used as initial values in Step 1 of the optimization procedure of Section II-D.) For each of the five test samples, we calculated the root-mean-square displacement error throughout all nodes on the boundaries of the five ellipses. These errors, normalized against the root-mean-square of the displacement vectors for the same nodes, are reported in Table I, together with the mean normalized error. Representative examples of the prediction of the deformed shapes are shown in Fig. 4(a) for SBE and Fig. 4(b) for FBE.

We then tested the performance of the algorithms on the set of samples with relatively higher variability in shape and mechanical parameters. Fig. 5 shows a representative result from that sample set. Here, FBE outperformed SBE. Error measurements are given in Table II.

B. Experiment 2

Our second experiment was motivated by the problem of modeling soft tissue deformation caused by tumor growth. In particular, in [5], we described a biomechanical model of brain deformation caused by tumor growth. Under certain approximations, we demonstrated that it is possible to model soft tissue deformation by tumor growth, and to use this model for matching an atlas of the human brain to a patient's images. One of the fundamental problems, however, in this type of modeling is that the patient's images prior to the development of the tumor are not available. The initial position in which the tumor started is not known, either. Therefore, it is practically not possible to model deformation imposed by tumor growth, knowing only the patient's images, unless oversimplifying approximations are made. Matching an atlas to a patient's images is also subject to the same problem, since the process of tumor growth and deformation of surrounding structures must be simulated on the atlas.

The ill posedness of the problem of tumor-induced deformation can be overcome by using the framework presented in this paper. In particular, one can build a statistical model linking shape and deformation, as we described in Section II, by selecting a number of normal brain images and simulating the deformation of soft tissue caused by the growth of a tumor. If a large number of such simulations are performed, then the resulting pairs of [shape, deformation] can be used in our framework to build a statistical model linking anatomy and deformation. Here, the anatomy is the patient's images, i.e., the anatomy deformed by the tumor. When new a patient's images are known, the deformation field can be estimated by our methodology. As an immediate result, the patient's anatomy prior to the development of the tumor can be estimated by applying the inverse deformation field. Finally, if an atlas of the normal brain is matched to the estimate of the patient's

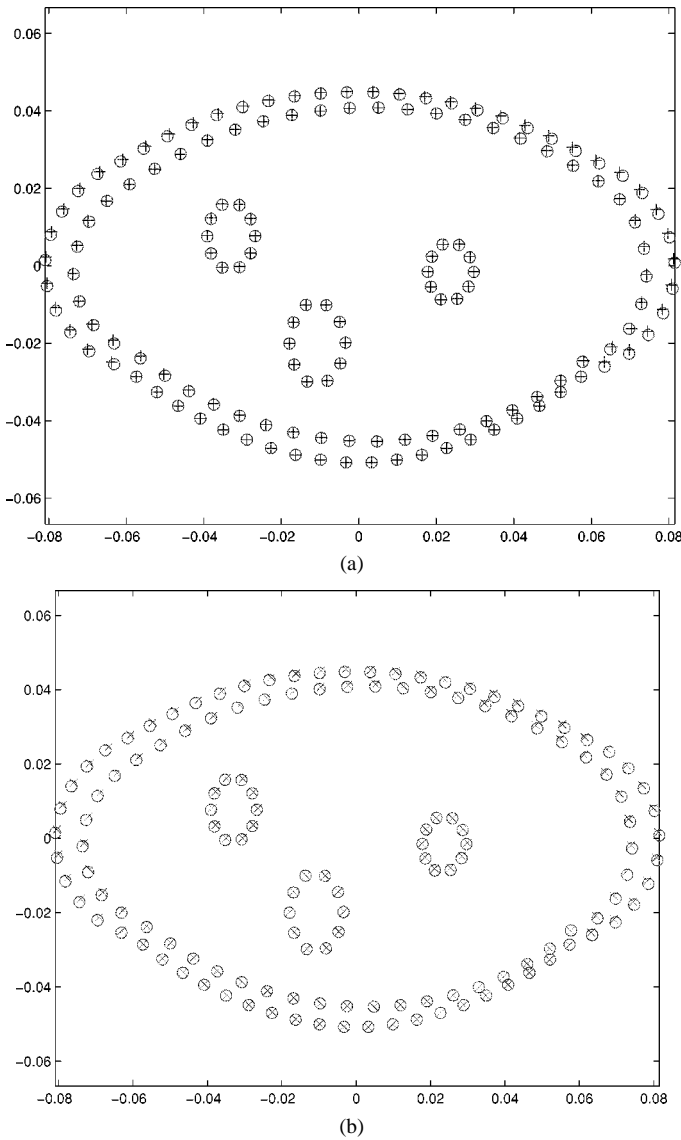


Fig. 4. Prediction of the deformation for test case 5 (last in Table I), for the set of 20 samples with relatively lower variability in shape and mechanical parameters. Circles denote the truth. (a) Result of SBE (crosses). (b) Result of FBE (Xs).

pretumor anatomy, it can then be mapped onto the patient’s images after tumor growth, for the purposes of surgical planning.

In order to test our framework in this paradigm, we generated 30 synthetic shapes representing the ventricles of different brains. We then deformed these shapes by growing tumors, as shown in Fig. 6. From the training samples we then calculated the mean and covariance matrix of \mathbf{x} , and the corresponding eigenvectors.

We then tested that, given the deformed configuration of a new shape, we could predict its undeformed configuration. Fig. 6 shows an example of this prediction mechanism. In Fig. 6(b), circles represent points of the deformed shape, and crosses represent the optimal fit found by minimizing the energy function in (5). Fig. 6(a) shows the predicted undeformed configuration of the shape, found by applying the inverse deformation field, along with true undeformed shape (in circles). The prediction was very accurate.

C. Computational Considerations

The most CPU intensive operation was the solution of the FE problems. Each solution needed an average of 2 minutes on a 225-MHz

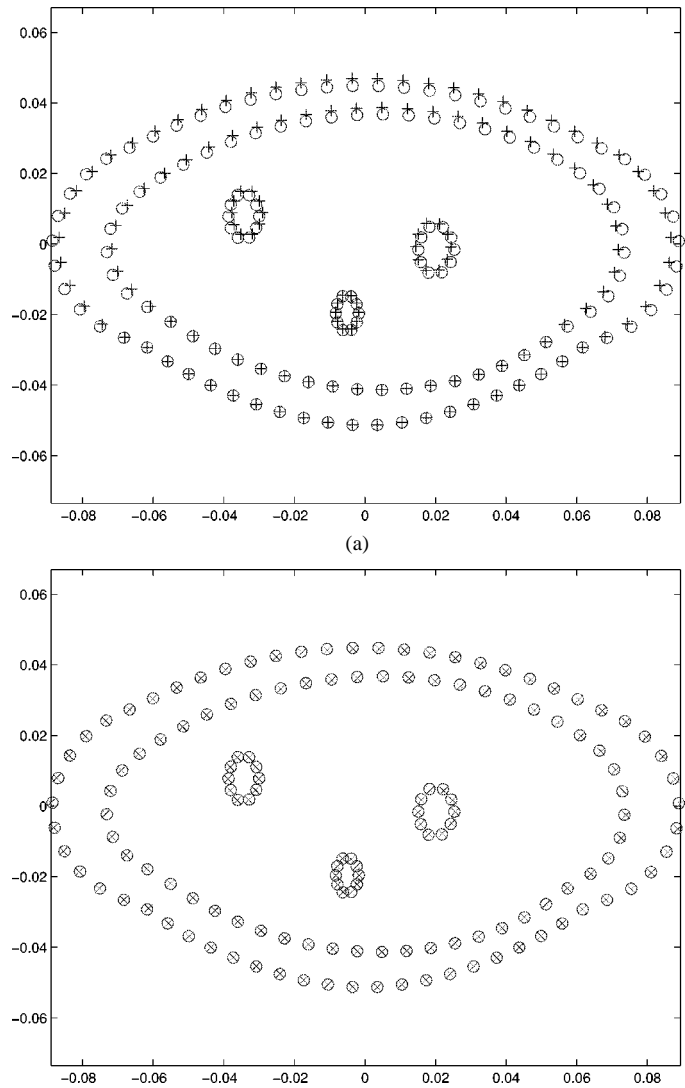


Fig. 5. Prediction of the deformation for test case 1 (first in Table II), for the set of 40 samples with relatively higher variability in shape and mechanical parameters. Circles denote the truth. (a) Result of SBE (crosses). (b) Result of FBE (Xs).

TABLE II
NORMALIZED ERRORS FROM VARIOUS TARGETS FOR THE TRAINING DATASET WITH THE RELATIVELY HIGHER PARAMETER VARIATION. THE MEAN FOR SBE WAS 0.3643 AND THE MEAN FOR FBE WAS 0.2257

Error in SBE	Error in FBE
0.304303	0.053248
0.126730	0.073419
0.346008	0.566100
0.532299	0.387028
0.512355	0.048511

Octane SGI with 128-MB RAM. In contrast, a statistical solution was on the order of 10 s. Note that FBE required the solution of a FE problem for each sample and the target so this method was slower than SBE by an order of magnitude.

In order to examine the error introduced in FBE by the inherently approximating nature of FE modeling, we tested the behavior of the two methods using a statistical sample set composed of 20 identical samples. SBE gave an error of 0.0000, as expected, while FBE gave an

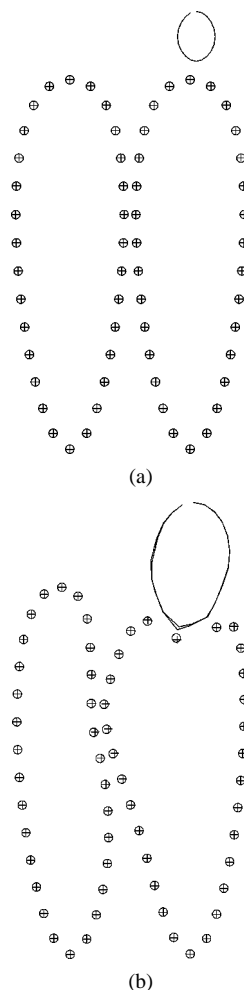


Fig. 6. Prediction of (a) the undeformed configuration from (b) the deformed configuration, from simulated data of tumor growth and deformation of surrounding shapes. Circles represent the true shapes and crosses represent the fitted (a) and predicted (b) shapes, using the proposed algorithm.

error of 0.0032. We conclude that the approximating nature of FEM is not a serious source of error in the methodology.

IV. DISCUSSION

We presented a methodological framework for predicting deformations, using information obtained from a training set. We examined two methods. The first method (SBE) is purely shape-based and it constructs a predictive model based on the primary modes of co-variation between anatomy and deformation. That is, it finds the component of deformation that can be predicted purely from knowledge of a patient's anatomy. The second method (FBE) utilizes knowledge about the biomechanical properties of the deforming anatomy, leaving the rest to a model analogous to the one used in SBE. Our preliminary results indicate that FBE outperforms SBE when large variations in anatomy, forces, and elastic parameters are present. However, both methods performed equally well under relatively lower variability. This is expected, since large deformation mechanics deviate from linearity, and therefore a linear statistical model should be expected to be relatively less accurate in that scenario.

FBE has the advantage that it utilizes knowledge about the biomechanical properties of anatomical structures. Moreover, it does not only estimate deformations on a discrete number of landmarks, but rather it determines a continuous displacement field. Its main drawback is the

additional computational complexity, which in three dimensions is expected to be considerable.

Although it is clearly impossible to fully predict intraoperative deformations without additional intraoperative data, it is certainly beneficial to predict as much as possible of the deformation, and to account for this deformation during preoperative planning. As preoperative plans might need to be adjusted and recomputed intraoperatively, starting from a good initial guess should substantially reduce optimal planning computational time.

Naturally, our model is capable of providing predictions which are limited to the aspects of the deformation that are systematic enough to be captured by the statistical model. For example, if we trained a statistical model to capture the deformation of a soft tissue body organ due to needle puncture, the model will only be capable of predicting deformations that are produced by needles inserted at the same point and with the same orientation as that which was encountered in the training cases. To overcome this limitation of the linear predictive statistical model, we are investigating the parameterization of the model by variables such as needle position and orientation. To be able to deal with problems of this nature, training should be performed separately for each value of the parameter (i.e., each possible orientation and insertion point of the needle).

Although in this paper we tested our proposed framework using simulations of fairly systematic anatomical deformations, our methodology has a very wide range of applications in real-time tracking of deformations. In particular, off-line biomechanical simulations can be used to train our statistical model, thus yielding a *statistical prior* for the kinds of deformations one would expect for the particular anatomy of the patient. This prior can then guide a real-time matching of preoperative images of the patient with limited intraoperative information, such as that provided by fluoroscopic or ultrasound images. Finally, interactions between surgical instruments and organs can be modeled the same way, after the statistical model is trained based on biomechanical simulations (e.g., simulations of needle puncturing). The gain of this approach is in speed, since biomechanical models are often too costly to be implemented in real time, whereas our statistical model can be updated very quickly on a regular PC.

On-going work focuses on the implementation in three dimensions, and on the application of this method in several clinical problems, in order to identify the applications which involve systematic deformations that can be predicted with reasonably high accuracy.

REFERENCES

- [1] O. M. Skrinjar and J. S. Duncan, "Real time 3-D brain shift compensation," in *Lecture Notes in Computer Science*, A. Kuba, M. Samal, and A. Todd-Pokropek, Eds. Berlin, Germany: Springer, vol. 1613, Proc. 16th Int. Conf. IPMI'99 (Information Processing in Medical Imaging), Visegrad, Hungary, June/July 1999.
- [2] K. D. Paulsen, M. I. Miga, F. E. Kennedy, P. J. Hoopes, A. Hartov, and D. W. Roberts, "A computational model for tracking subsurface tissue deformation during stereotactic neurosurgery," *IEEE Trans. Biomed. Eng.*, vol. 46, pp. 213–225, Feb. 1999.
- [3] C. R. Maurer Jr., D. L. G. Hill, A. J. Martin, H. Liu, M. McCue, D. Rueckert, D. Lloret, W. A. Hall, R. E. Maxwell, D. J. Hawkes, and C. L. Truitt, "Investigation of intraoperative brain deformation using a 1.5-T interventional MR system: Preliminary results," *IEEE Trans. Med. Imag.*, vol. 17, pp. 817–825, Oct. 1998.
- [4] K. Müller, K. Chinzei, G. Orsengo, and P. Bednarz, "Mechanical properties of brain tissue in-vivo: Experiment and computer simulation," *J. Biomech.*, vol. 33, pp. 1369–1376, 2000.
- [5] S. K. Kyriacou, C. Davatzikos, S. J. Zinreich, and R. N. Bryan, "Non-linear elastic registration of brain images with tumor pathology using a biomechanical model," *IEEE Trans. Med. Imag.*, vol. 18, pp. 580–592, July 1999.
- [6] R. M. Wasserman, R. S. Acharya, C. Sibata, and K. H. Shin, "Patient-specific tumor prognosis prediction via multimodality imaging," in *Proc. SPIE Int. Soc. Optical Engineering*, 1996, p. 2709.

- [7] T. Nagashima, T. Shirakuni, and S. I. Rapoport, "A two-dimensional, finite element analysis of vasogenic brain edema," *Neurologia Medico-Chirurgica*, vol. 30, no. 1, pp. 1–9, 1990.
- [8] T. Nagashima, N. Tamaki, M. Takada, and Y. Tada, "Formation and resolution of brain edema associated with brain tumors. A comprehensive theoretical model and clinical analysis," *Acta Neurochirurgica: Supplementum (Wien)*, vol. 60, pp. 165–167, 1994.
- [9] Y. Tada, T. Nagashima, and M. Takada, "Biomechanics of brain tissue (simulation of cerebrospinal fluid flow)," *JSME Int. J.*, ser. A, vol. 37, no. 2, pp. 188–194, 1994.
- [10] R. P. Subramaniam, S. R. Neff, and P. Rahulkumar, "A numerical study of the biomechanics of structural neurologic diseases," in *Proc. High Performance Computing-Grand Challenges in Computer Simulation Society for Computer Simulations*, A. Tentner, Ed., San Diego, CA, 1995, pp. 552–560.
- [11] M. Kaczmarek, R. P. Subramaniam, and S. R. Neff, "The hydromechanics of hydrocephalus: Steady-state solutions for cylindrical geometry," *Bull. Math. Biol.*, vol. 59, pp. 295–323, 1997.
- [12] H. Takizawa, K. Sugiura, M. Baba, and J. D. Miller, "Analysis of intracerebral hematoma shapes by numerical computer simulation using the finite element method," *Neurologia Medico-Chirurgica*, vol. 34, pp. 65–69, 1994.
- [13] K. Voo, S. Kumaresan, F. A. Pintar, N. Yoganandan, and A. Sances Jr., "Finite-element models of the human head," *Med. Biol. Eng. Comput.*, vol. 34, no. 5, pp. 375–381, 1996. Review.
- [14] F. A. Bandak, M. J. Vander Vorst, L. M. Stuhmiller, P. F. Mlakar, W. E. Chilton, and J. H. Stuhmiller, "An imaging-based computational and experimental study of skull fracture: Finite element model development," *J. Neurotrauma*, vol. 12, no. 4, pp. 679–688, 1995. Review.
- [15] A. H. Kuijpers, M. H. Claessens, and A. A. Sauren, "The influence of different boundary conditions on the response of the head to impact: A two-dimensional finite element study," *J. Neurotrauma*, vol. 12, no. 4, pp. 715–724, 1995.
- [16] A. I. King, J. S. Ruan, C. Zhou, W. N. Hardy, and T. B. Khalil, "Recent advances in biomechanics of brain injury research: A review," *J. Neurotrauma*, vol. 12, no. 4, pp. 651–658, 1995.
- [17] K. Ueno, J. W. Melvin, L. Li, and J. W. Lighthall, "Development of tissue level brain injury criteria by finite element analysis," *J. Neurotrauma*, vol. 12, no. 4, pp. 695–706, 1995.
- [18] S. Kumaresan and S. Radhakrishnan, "Importance of partitioning membranes of the brain and the influence of the neck in head injury modeling," *Med. Biol. Eng. Comput.*, vol. 34, no. 1, pp. 27–32, 1996.
- [19] B. R. Donnelly and J. Medige, "Shear properties of human brain tissue," *J. Biomech. Eng.*, vol. 119, no. 4, pp. 423–432, 1997.
- [20] H. Metz, J. McElhaney, and A. K. Ommaya, "A comparison of the elasticity of live, dead, and fixed brain tissue," *J. Biomech.*, vol. 3, pp. 453–458, 1970.
- [21] K. K. Mendis, R. Stalnaker, and S. H. Advani, "A constitutive relationship for large-deformation finite-element modeling of brain-tissue," *J. Biomech. Eng. Trans. ASME*, vol. 117, pp. 279–285, 1995.
- [22] L. E. Bilston and L. E. Thibault, "The mechanical properties of the human cervical spinal cord in vitro," *Ann. Biomed. Eng.*, vol. 24, pp. 67–74, 1996.
- [23] S. S. Margulies, L. E. Thibault, and T. A. Gennarelli, "Physical model simulations of brain injury in the primate," *J. Biomech.*, vol. 23, no. 8, pp. 823–836, 1990.
- [24] K. Miller and K. Chinzei, "Constitutive modeling of brain tissue—experiment and theory," *J. Biomech.*, vol. 30, pp. 1115–1121, 1997.
- [25] S. K. Kyriacou, D. Shen, and C. Davatzikos, "A framework for predictive modeling of intraoperative deformations: A simulation-based study," presented at the Medical Image Comput. and Computer Assisted Interventions in Medicine, MICCAI'2000, Oct. 2000.
- [26] P. R. Anderson, F. L. Bookstein, K. Conradsen, B. K. Ersboll, J. L. Marsh, and S. Kreiborg, "Surface-bounded growth modeling applied to human mandibles," *IEEE Trans. Med. Imag.*, vol. 19, pp. 1053–1063, Nov. 2000.
- [27] F. T. Cootes and C. J. Taylor, "Combining point distribution models with shape models based on finite element analysis," *Image Vis. Comput.*, vol. 13, no. 5, pp. 403–409, 1995.
- [28] M. I. Miller, G. E. Christensen, Y. Amit, and U. Grenander, "Mathematical textbook of deformable neuroanatomies," in *Proc. Nat. Acad. Sci.*, vol. 90, 1993, pp. 11 944–11 948.
- [29] D. Shen, E. Herskovits, and C. Davatzikos, "Segmentation and shape modeling of 3D MR structures using an adaptive focus statistical shape model," *IEEE Trans. Med. Imag.*, vol. 20, Mar. 2001.

- [30] A. Kelemen, G. Szekely, and G. Gerig, "Elastic model-based segmentation of 3-D neuroradiological data sets," *IEEE Trans. Med. Imag.*, vol. 18, pp. 828–839, Oct. 1999.
- [31] D. Shen and C. Davatzikos, "An adaptive focus deformable model using statistical and geometric information," *IEEE Trans. Pattern Anal. Machine Intell.*, vol. 22, pp. 906–913, 2000.
- [32] D. W. Marquardt, "An algorithm for least-squares estimation of non-linear parameters," *J. Soc. Ind. Appl. Math.*, vol. 11, p. 431, 1963.
- [33] "Abaqus Version 6.1," Hibbit, Karlsson, and Sorensen, Inc., Pawtucket, RI, 2000.

A Bound on Mutual Information for Image Registration

Mark B. Skouson, Quji Guo, and Zhi-Pei Liang*

Abstract—An upper bound is derived for the mutual information between a fixed image and a deformable template containing a fixed number of gray-levels. The bound can be calculated by maximizing the entropy of the template under the constraint that the conditional entropy of the template, given the fixed image, be zero. This bound provides useful insight into the properties of mutual information as a similarity metric for deformable image registration. Specifically, it indicates that maximizing mutual information may not necessarily produce an optimal solution when the deformable transform is too flexible.

Index Terms—Deformation, information bound, mutual information, registration.

I. INTRODUCTION

Mutual information (MI) has been used as a similarity metric in several areas of signal processing, including estimation of time delays in electroencephalogram signals [1], image registration [2], [3], and image deformation [4]–[6]. Several of its properties have been studied, including bias and variance analysis [7] and interpolation effects [8]. This paper derives an upper bound on the maximum MI achievable for deformable image registration. This bound should provide further insight into the use of MI as a similarity metric.

II. BACKGROUND

Let A and B be two discrete random variables with outcomes from sample spaces Ω_A and Ω_B , respectively. Their mutual information is [9]

$$I(A; B) = \sum_{a \in \Omega_A} \sum_{b \in \Omega_B} P_{AB}(a, b) \log \frac{P_{AB}(a, b)}{P_A(a)P_B(b)} \quad (1)$$

Manuscript received June 13, 2000; revised May 22, 2001. This work was supported in part by the National Science Foundation (NSF) under Grant BES-95-02 121 and in part by the National Institutes of Health (NIH) under Grant R21-HL062 336. The Associate Editor responsible for coordinating the review of this paper and recommending its publication was C. R. Meyer. *Asterisk indicates corresponding author.*

M. B. Skouson and Q. Guo are with the Department of Electrical and Computer Engineering and The Beckman Institute for Advanced Science and Technology, University of Illinois at Urbana-Champaign, Urbana, IL 61801 USA.

*Z.-P. Liang is with the Department of Electrical and Computer Engineering and The Beckman Institute for Advanced Science and Technology, University of Illinois at Urbana-Champaign, 1406 West Green Street, Urbana, IL 61801 USA (e-mail: z-liang@uiuc.edu).

Publisher Item Identifier S 0278-0062(01)06588-0.